Exact Results for a Semiflexible Polymer Chain in an Aligning Field

Andrew J. Spakowitz and Zhen-Gang Wang*

Division of Chemistry and Chemical Engineering, California Institute of Technology, Pasadena, California 91125

Received January 5, 2004; Revised Manuscript Received April 23, 2004

ABSTRACT: We provide exact results for the Laplace-transformed partition function of a wormlike chain subject to a tensile force and in a nematic field, in both two and three dimensions. The results are in the form of infinite continued fractions, which are obtained by exploiting the hierarchical structure of a moment-based expansion of the partition function. The case of an imaginary force corresponds to the end-to-end distance distribution in Laplace−Fourier space. We illustrate the utility of these exact results by examining the structure factor of a wormlike chain, the deformation free energy of a chain in a nematic field, and the self-consistent-field solution for the isotropic−nematic transition of wormlike chains.

1. Introduction

A number of physical problems involving semiflexible polymers can be mapped to that of a single chain in an external field. The force−extension behavior of a single semiflexible polymer is described as the response of a polymer to a dipole aligning field acting on the end-to-end distance vector.[1−4] The behavior of a semiflexible chain dissolved in a nematic liquid crystal corresponds to a polymer in a quadrupole aligning field.[5] The latter problem also naturally arises in the self-consistent-field description of polymer liquid crystals.[6−9] Perhaps less obvious, finding the end-to-end distance distribution function of a polymer involves solving for the partition function of a chain in an imaginary dipole field.[10−12] Since these problems share a similar mathematical representation, methods for studying the behavior of a semiflexible chain in an external aligning field have many applications in polymer physics.

In this paper, we provide exact analytical solutions for the partition function in Laplace space of a wormlike polymer subject to real and imaginary dipole fields and a nematic quadrupole field, in both two and three dimensions, and use these results to examine the structure factor, the deformation free energy of a polymer chain in a nematic liquid crystal, and the self-consistent-field solution for the isotropic−nematic transition of wormlike chains. The methods employed in this work rely on the use of the diagrammatic representation of Yamakawa[10] for the moments of the end-to-end distance distribution function. By exploiting the hierarchical structure of the moment expansion of the various partition functions, we are able to re-sum the infinite diagrammatic series into a simple, exact, and concise continued-fraction form. We note that the end-to-end distance distribution for the wormlike chain model was recently obtained by two groups. Samuel and Sinha provided a numerical solution by a direct diagonalization of the truncated scattering matrix.[11] Stepanow and Schütz obtained exact results[12] using algebraic techniques developed by Temperley and Lieb in their study of graph-theoretical problems involving regular planar lattices.[13] However, our results are advantageous by virtue of their simple and compact analytical structure which makes them convenient to use. In addition, our re-summation method is applicable to a single chain in a nematic field, a helical wormlike chain, and a class of physical problems including a quantum-mechanical rigid rotor and a Brownian particle undergoing rotational diffusion.

The rest of this paper is organized as follows. In section II, we discuss our analytical solutions in two dimensions with a detailed explanation of the method. In section III, we present the analogous three-dimensional solutions and provide a discussion on the generalization of our techniques. In section IV, we use our result for the end-to-end distance distribution function to study the structure factor of a wormlike chain. In section V, we discuss the deformation of a wormlike chain in a nematic liquid crystal and the self-consistent-field free energy of polymer liquid crystals in conjunction with our earlier work on the subject.[9] Finally, we conclude with a summary of our results in section VI.

2. Two-Dimensional Solutions

The wormlike chain model in d dimensions is described by an inextensible space curve $\vec{r}(s)$ parametrized by the path length coordinate s that runs from zero to the contour length of the chain L. The inextensibility is enforced by constraining the tangent vector $\vec{u} \equiv \partial_s \vec{r}$ such that $|\vec{u}| = 1$ for all s. The bending deformation energy, which is quadratic in the curvature of the space curve, is given by[14]

$$\beta\mathscr{H}_0 = \frac{l_p}{2}\int_0^L \mathrm{d}s \left(\frac{\partial \vec{u}}{\partial s}\right)^2 \tag{1}$$

where l_p is the persistence length and $\beta = 1/(k_B T)$. The total chain Hamiltonian is given by $\beta\mathscr{H} = \beta\mathscr{H}_0 + \beta\mathscr{H}_{ext}$, where $\beta\mathscr{H}_{ext}$ represents the interaction between the polymer chain and the external field.

In two dimensions, the orientation of the tangent vector is defined by the angle θ between the tangent and the x-axis of an arbitrarily chosen coordinate system. The orientational statistics of the wormlike chain in the absence of an external field is described by the Green function $G_0(\theta|\theta_0;L)$ defined to be the conditional probability that a chain of length L with initial orientation angle θ_0 will have the final orientation angle θ. The Green function is found by summing over the

10.1021/ma049958v CCC: $27.50
Published on Web 06/22/2004

paths between θ_0 and θ, giving each path the amplitude $\exp(-\beta\mathscr{H}_0)$, which is formally stated as

$$G_0(\theta|\theta_0;L) = \int_{\theta(s=0)=\theta_0}^{\theta(s=L)=\theta} \mathscr{D}[\theta(s)]\exp(-\beta\mathscr{H}_0[\theta(s)]) \quad (2)$$

where $\mathscr{D}[\theta(s)]$ indicates path integration over the fluctuating field $\theta(s)$.

The formal statement of $G_0(\theta|\theta_0;L)$ (eq 2) reflects the correspondence between the Green function of the wormlike chain model and the quantum-mechanical propagator of a quantum particle confined to a unit circle;[15] our current problem corresponds to finding the propagator of a quantum particle confined to a unit circle with the bending energy playing the role of the kinetic energy and the contour length acting as an imaginary time. Using this quantum-mechanical analogy, the Green function can be written as an eigenfunction expansion

$$G_0(\theta|\theta_0;L) = \sum_{m=-\infty}^{\infty} \frac{1}{2\pi} e^{im(\theta-\theta_0)} \exp\left(-\frac{m^2 L}{2l_p}\right) \quad (3)$$

With this background, we now consider the partition function of a wormlike chain subject to a tensile force $\vec{f}$ acting on the end-to-end distance vector $\vec{R} \equiv \int_0^L \mathrm{d}s\ \vec{u}$. The interaction due to this force is accounted for by $\beta\mathscr{H}_{\mathrm{ext}} = -\vec{f}\cdot\int_0^L \mathrm{d}s\ \vec{u}$. Without loss of generality, we assume the force to be aligned along the x-axis. The partition function of the chain $q(f;L)$ relative to that of the free chain is now given by

$$q(f;L) = \langle \exp(fR_x)\rangle_0 = \sum_{n=0}^{\infty} \frac{f^{2n}}{(2n)!}\langle R_x^{2n}\rangle_0 \quad (4)$$

where f is the magnitude of $\vec{f}$, and $\langle ...\rangle_0$ indicates an average taken with respect to $\beta\mathscr{H}_0$ (eq 1). We note that the second form of eq 4 excludes the odd moments of R_x because of the rotational invariance of $\beta\mathscr{H}_0$. The first form of $q(f;L)$ in eq 4 might suggest that the solution technique would be a cumulant expansion of the argument of the exponential; however, a cumulant expansion is rapidly convergent only for statistics that are close to Gaussian, which is not the case for the wormlike chain model. The second form of $q(f;L)$ in eq 4 is the so-called moment-based expansion,[10] which we proceed to exploit.

Using $R_x = \int_0^L \cos\theta(s)$, we write the moments $\langle R_x^{2n}\rangle_0$ in the following form

$$\langle R_x^{2n}\rangle_0 = (2n)!\,\langle \prod_{i=1}^{2n} \int_0^{s_{i-1}} \mathrm{d}s_i \cos\theta(s_i)\rangle_0 \quad (5)$$

where $s_0 = L$, and the factor of $(2n)!$ comes from the "time" ordering of the integrations. Taking advantage of the Markovian nature of the orientation statistics, we evaluate the above average by inserting a propagator (eq 3) between successive factors in the product on the right-hand side of eq 5 and integrating over the initial, final, and intermediate orientations. For $\langle R_x^{2n}\rangle_0$, there are $2n + 1$ propagators and thus $2n + 1$ m-indices to sum over.

The summation over the m-indices after integration over the angular variables is greatly simplified because of the completeness and orthogonality of the eigenfunctions $e^{im\theta}$. The integration over the initial and final orientations results in setting the first and last m-indices to zero. Since $\cos\theta e^{im\theta} = e^{i(m+1)\theta}/2 + e^{i(m-1)\theta}/2$, the intermediate m-indices that make nonzero contributions to the average are selected by the criteria that they are offset from their neighbors by either $+1$ or -1. As an example, we consider $\langle R_x^2\rangle_0$, which contains three m-indices from three propagators. Performing the average, we have

$$\langle R_x^2\rangle_0 = \frac{1}{2}\int_0^L \mathrm{d}s_1 \int_0^{s_1} \mathrm{d}s_2 \sum_{m_1,m_2,m_3} \delta_{0,m_1} C_{m_1}(L - s_1) \times (\delta_{m_1,m_2+1} + \delta_{m_1,m_2-1}) C_{m_2}(s_1 - s_2) \times (\delta_{m_2,m_3+1} + \delta_{m_2,m_3-1}) C_{m_3}(s_2)\delta_{m_3,0} \quad (6)$$

where the summations over the m-indices run from negative infinity to infinity, $\delta_{m,n}$ is the Kronecker delta function, and $C_m(L) = \exp[-m^2 L/(2l_p)]$. Performing the summations over the m-indices leaves only two sets of values that contribute to the average: ($m_1 = 0$, $m_2 = 1$, $m_3 = 0$) and ($m_1 = 0$, $m_2 = -1$, $m_3 = 0$). These two sets of m-indices satisfy the previously mentioned selection criteria; the selected m-indices are offset from their neighbors by either 1 or -1 with starting and ending values of zero.

We now generalize the calculation to $\langle R_x^{2n}\rangle_0$. Using eq 5 with the solution for the propagator (eq 3), the value of a given moment is

$$\langle R_x^{2n}\rangle_0 = \frac{(2n)!}{2^{2n}} \prod_{i=1}^{2n} \sum_{\{m_i\}} \delta_{0,m_1} \int_0^{\tau_{i-1}} d\tau_i C_{m_i}(\tau_{i-1} - \tau_i) \times (\delta_{m_i,m_{i+1}+1} + \delta_{m_i,m_{i+1}-1})\delta_{m_{2n+1},0} C_{m_{2n+1}}(\tau_{2n}) \quad (7)$$

where $\tau = s/(2l_p)$ [$\tau_0 = N \equiv L/(2l_p)$], the sum over $\{m_i\}$ indicates summation over all m_i ($i = 1, 2, ..., 2n + 1$) from negative infinity to infinity, and we have nondimensionalized R_x by $2l_p$. Evaluating eq 7 involves finding the values of the $2n + 1$ m-indices that are selected by the Kronecker delta functions upon summing over the m-index values. Essentially, this task involves finding the m-index values that correspond to paths between zero and zero with $2n$ steps of unit magnitude in between. Performing a Laplace transform of eq 7 from N to p, we have

$$\mathscr{L}(\langle R_x^{2n}\rangle_0) = \frac{(2n)!}{2^{2n}} \prod_{i=1}^{2n} \sum_{\{m_i\}} \delta_{0,m_1} \frac{1}{P_{m_i}} \frac{1}{P_{m_{2n+1}}} \times (\delta_{m_i,m_{i+1}+1} + \delta_{m_i,m_{i+1}-1})\delta_{m_{2n+1},0} \quad (8)$$

where $\mathscr{L}$ indicates a Laplace transform from N to p, and $P_m = p + m^2$, which arises from the convolution present in eq 7. The form of eq 8 indicates that our current problem involves algebraically summing the terms that contribute to the moment by finding the m-index paths that result in nonzero contributions upon summing over the m-indices.

The selected m-index paths can be expressed diagrammatically using a stone-fence representation proposed by Yamakawa;[10] in Figure 1, we provide the diagrams that contribute to the calculation of $\langle R_x^4\rangle_0$ (A) and $\langle R_x^6\rangle_0$ (B). These diagrams show all the possible m-index combinations that run from zero to zero while following the intermediate selection rules for these two

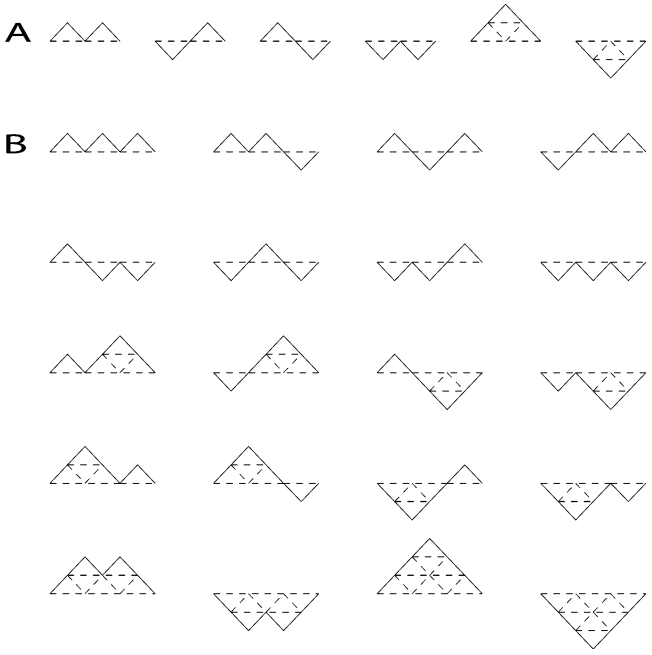

Figure 1. Stone-fence diagrams contributing to the calculation of $\langle R_x^4 \rangle$ (A) and $\langle R_x^6 \rangle$ (B) in two dimensions.

moments. For example, the first diagram in A of Figure 1 corresponds to m-index values of ($m_1 = 0$, $m_2 = 1$, $m_3 = 0$, $m_4 = 1$, $m_5 = 0$), giving an algebraic contribution $P_0^{-3} P_1^{-2}$ to the Laplace transform of $\langle R_x^4 \rangle_0$. Since the moment $\langle R_x^{2n} \rangle_0$ contains $2n + 1$ m-indices and thus $2n$ intermediate steps, contributing diagrams require an equal number (n) of up and down steps to run from zero to zero. As a result, $\langle R_x^{2n} \rangle_0$ contains $(2n)!/(n!)^2$ distinct diagrams, which is the number of ways of distributing n up steps and n down steps in $2n$ total steps.

Using eq 8, we restate eq 4 in Laplace space as

$$q(F;p) = \sum_{n=0}^{\infty} \left(\frac{F}{2}\right)^{2n} \sum_{\text{paths } \mu}^{0 \to 0} \prod_{i=1}^{2n+1} \frac{1}{P_{m_i(\mu)}} \tag{9}$$

where $F = 2l_p f$ and the summation over the paths μ implies a summation over all available stone-fence diagrams of $2n$ steps starting and ending at $m = 0$. Equation 9 as it stands groups the diagrams according to the number of m-indices they contain, where the nth term in the expansion contains diagrams with $2n + 1$ m-indices. Evaluation of eq 9 in this manner is a formidable task since all diagrams for each order n must be explicitly calculated, and the number of diagrams increases exponentially with n [as $(2n)!/(n!)^2$].

We now develop a re-summation technique for evaluating eq 9 by re-grouping the diagrams. To this end, we modify the definition of the stone-fence diagrams by absorbing the factor $(F/2)^{2n}$ into the diagrams. In the modified stone-fence diagrams, each m-index is associated with a factor $P_m^{-1} = (p + m^2)^{-1}$ and each step is associated with a factor $F/2$. Henceforth we will refer to these modified diagrams as F diagrams. In terms of these F diagrams, eq 9 can be written as

$$q(F;p) = \text{sum of all F diagrams that begin and terminate at } m = 0 \tag{10}$$

The full set (infinite number) of F diagrams can be classified according to the number of intermediate m-indices that are zero; thus

$$\begin{aligned} q(F;p) = {} & \text{the diagram with a single } m = 0 \text{ index} + \\ & \text{sum of all F diagrams that begin and terminate at } m = 0 \text{ with no intermediate zero-valued } m\text{-indices} + \\ & \text{sum of all F diagrams that begin and terminate at } m = 0 \text{ with one intermediate zero-valued } m\text{-index} + \\ & \text{sum of all F diagrams that begin and terminate at } m = 0 \text{ with two intermediate zero-valued } m\text{-indices} + \ldots \\ = {} & P_0^{-1} + q^{(1)} + q^{(2)} + q^{(3)} + \ldots \end{aligned} \tag{11}$$

The ellipsis within eq 11 indicates that $q(F;p)$ is recast as an infinite summation of $q^{(l)}$, where $q^{(l)}$ represents the infinite sum of F diagrams that begin and terminate at $m = 0$ with $l - 1$ intermediate zero-valued m-indices.

The diagrams within the first subset of F diagrams ($q^{(1)}$) fall into two categories: diagrams that start and end at $m = 0$ by going through positive values of m and diagrams that start and end at $m = 0$ by going through negative values of m. The diagrams within the first category can be written as

$$\frac{1}{P_0}\frac{F}{2} w_1 \frac{F}{2}\frac{1}{P_0} = P_0^{-2}\left(\frac{F^2}{4}\right) w_1 \tag{12}$$

where w_1 represents all diagrams beginning and terminating at $m = 1$ with no intermediate m-indices below 1. Similarly, the diagrams within the second category can be written as

$$\frac{1}{P_0}\frac{F}{2} w_{-1} \frac{F}{2}\frac{1}{P_0} = P_0^{-2}\left(\frac{F^2}{4}\right) w_{-1} \tag{13}$$

where w_{-1} represents all diagrams beginning and terminating at $m = -1$ with no intermediate m-indices above -1. Thus,

$$q^{(1)}(F;p) = P_0^{-2}\left(\frac{F^2}{4}\right)(w_1 + w_{-1}) \tag{14}$$

We can now express the diagrams in each group using the functions w_1 and w_{-1}. Some reflection should convince the reader that the sum of all F diagrams that begin and terminate at $m = 0$ with one intermediate zero-valued m-index ($q^{(2)}$) can be written as

$$\begin{aligned} q^{(2)}(F;p) = {} & P_0^{-1}\frac{F}{2} w_1 \frac{F}{2} P_0^{-1}\frac{F}{2} w_1 \frac{F}{2} P_0^{-1} + \\ & P_0^{-1}\frac{F}{2} w_{-1} \frac{F}{2} P_0^{-1}\frac{F}{2} w_{-1} \frac{F}{2} P_0^{-1} + \\ & P_0^{-1}\frac{F}{2} w_1 \frac{F}{2} P_0^{-1}\frac{F}{2} w_{-1} \frac{F}{2} P_0^{-1} + \\ & P_0^{-1}\frac{F}{2} w_{-1} \frac{F}{2} P_0^{-1}\frac{F}{2} w_1 \frac{F}{2} P_0^{-1} \\ = {} & P_0^{-3}\left(\frac{F^2}{4}\right)^2 (w_1 + w_{-1})^2 \end{aligned} \tag{15}$$

Generalizing this to $q^{(l)}$, we obtain

$$q^{(l)}(F;p) = P_0^{-l-1}\left(\frac{F^2}{4}\right)^l (w_1 + w_{-1})^l \tag{16}$$

In terms of w_1 and w_{-1}, eq 9 can now be written as

$$q(F;p) = \sum_{l=0}^{\infty}\left(\frac{F^2}{4}\right)^l \frac{(w_1 + w_{-1})^l}{P_0^{\,l+1}} = \sum_{l=0}^{\infty}\left(\frac{F^2}{4}\right)^l \frac{(2w_1)^l}{P_0^{\,l+1}} = \frac{1}{P_0 - F^2 w_1/2} \tag{17}$$

where the second form is due to the equivalence between w_1 and w_{-1} (since $P_j = P_{-j}$). Describing eq 17 in words, we have performed a re-summation of eq 9 by collecting all diagrams that contain the same number of intermediate zero-valued m-indices and collapsing the sum of diagrams between adjacent zero-valued m-indices into the function w_1 for diagrams that remain above zero and the function w_{-1} for diagrams that remain below zero.

A similar classification scheme to the one we have used to write $q(F;p)$ can be developed for the functions w_1 and w_{-1}. For example,

w_1 = the diagram with a single $m = 1$ index + sum of all F diagrams that begin and terminate at $m = 1$ with all intermediate m-indices above 1 + sum of all F diagrams that begin and terminate at $m = 1$ with one intermediate m-index equal 1 and all other intermediate m-indices above 1 + sum of all F diagrams that begin and terminate at $m = 1$ with two intermediate m-indices equal 1 and all other intermediate m-indices above 1 + ...

$$= P_1^{-1} + w_1^{(1)} + w_1^{(2)} + w_1^{(3)} + \ldots \tag{18}$$

The ellipsis within eq 18 indicates that w_1 is recast as an infinite summation of $w_1^{(l)}$, where $w_1^{(l)}$ represents the infinite sum of F diagrams that begin and terminate at $m = 1$ with $l - 1$ intermediate m-indices equal 1 and all other intermediate m-indices above 1. Introducing w_2 as the infinite sum of all F diagrams that begin and terminate at $m = 2$ with no intermediate m-indices below 2, w_1 can be written as

$$w_1 = P_1^{-1} + P_1^{-1}\frac{F}{2}w_2\frac{F}{2}P_1^{-1} + P_1^{-1}\frac{F}{2}w_2\frac{F}{2}P_1^{-1}\frac{F}{2}w_2\frac{F}{2}P_1^{-1} + \ldots = \sum_{l=0}^{\infty}\left(\frac{F^2}{4}\right)^l \frac{w_2^{\,l}}{P_1^{\,l+1}} = \frac{1}{P_1 - F^2 w_2/4} \tag{19}$$

In general, if we define w_j as the infinite sum of all F diagrams that begin and terminate at $m = j$ with no intermediate m-indices below j (for positive j's), we obtain the following recursive relation:

$$w_j = \sum_{l=0}^{\infty}\left(\frac{F^2}{4}\right)^l \frac{w_{j+1}^{\,l}}{P_j^{\,l+1}} = \frac{1}{P_j - F^2 w_{j+1}/4} \tag{20}$$

where $P_j = p + j^2$. For negative j's, w_{j+1} in the above equation should be replaced by w_{j-1}. The recursive form reflects a hierarchical self-similarity in the relationship between the summation of diagrams at a given level with the summation of diagrams at the next level.

Equation 17 can be equivalently written as $q(F;p) = 1/[P_0 - (F^2/2)/J_1]$ with the recursive relation $J_n = P_n - (F^2/4)/J_{n+1}$ ($n \geq 1$). Repeated use of the recursive relation leads to an infinite continued fraction representation of the partition function of a wormlike chain under tension:

$$q(F;p) = \cfrac{1}{P_0 - \cfrac{F^2/2}{P_1 - \cfrac{F^2/4}{P_2 - \cfrac{F^2/4}{P_3 - \cfrac{F^2/4}{\cdots}}}}} \tag{21}$$

The emergence of the continued fraction form of eq 21 is a natural manifestation of the self-similarity of the summation of diagrams at different levels. The extra factor of 2 at the zeroth level of eq 21 is due to the equivalence between P_m and P_{-m}; the denominator of eq 21 can be equivalently written as a continued fraction to positive infinity plus a continued fraction to negative infinity.

The partition function $q(F;L)$ can be used to describe the thermodynamic behavior of a wormlike chain under tension. In particular, the derivatives of the partition function with respect to the force yields moments of the end-to-end distance in the direction of the force:

$$\langle R_x^{\,n}\rangle = \frac{1}{q}\frac{\mathrm{d}^n q}{\mathrm{d}F^n} \tag{22}$$

where R_x is nondimensionalized by $2l_p$. Of special interest is the first moment, which gives the force−extension behavior of the chain.

When the derivatives in eq 22 are evaluated at $F = 0$, we obtain the moments of the end-to-end distribution in the absence of the force. Inspection of eq 4 shows that $q(F;L)$ acts as a moment-generating function, i.e.,

$$\langle R_x^{\,2n}\rangle_0 = \left.\frac{\mathrm{d}^{2n} q}{\mathrm{d}F^{2n}}\right|_{F=0} \tag{23}$$

Using the relationship in two dimensions $\langle R^{2n}\rangle_0 = (n!)^2 4^n \langle R_x^{2n}\rangle_0/(2n)!$, eq 21 provides a convenient means for calculating moments of the end-distribution function without the laborious efforts of enumerating and computing all the stone-fence diagrams that contribute to a moment of a given order. Equation 23 also provides an easy way of verifying the validity of eq 21. We have computed moments up to $\langle R^{10}\rangle_0$ using eq 23 and find perfect agreement with the known solutions.[16]

We now consider the end-to-end distribution function $G(\vec{R};L)$, which gives the probability that a chain that begins at the origin will have end position $\vec{R}$, independent of the initial and final tangential orientations. $G(\vec{R};L)$ can be written as

$$G(\vec{R};L) = \langle \delta(\vec{R} - \int_0^L \mathrm{d}s\, \vec{u}) \rangle_0 \tag{24}$$

where $\langle ... \rangle_0$ indicates an average taken with respect to the unperturbed Hamiltonian $\beta\mathscr{H}_0$. Upon Fourier transforming from the variable $\vec{R}$ to $\vec{k}$, our problem becomes that of a single wormlike chain in the external dipole field $i\vec{k}$; thus $\beta\mathscr{H}_{\mathrm{ext}} = -i\vec{k}\cdot\int_0^L \mathrm{d}s\, \vec{u}$. The form of $\beta\mathscr{H}_{\mathrm{ext}}$ is identical to that for the chain under a tensile force $\vec{f}$ with $\vec{f} \rightarrow i\vec{k}$. Aligning $\vec{k}$ along the x-axis and defining $K \equiv 2l_p k$, where k is the magnitude of $\vec{k}$, the Laplace−Fourier transformed end-to-end distribution can be trivially obtained from eq 21 by replacing F^2 with $-K^2$; the result is

$$G(K;p) = \cfrac{1}{P_0 + \cfrac{K^2/2}{P_1 + \cfrac{K^2/4}{P_2 + \cfrac{K^2/4}{P_3 + \cfrac{K^2/4}{\cdots}}}}} \tag{25}$$

The end-to-end distribution function $G(R;L)$ can be obtained by an inverse Laplace−Fourier transform.

Finally, we consider the partition function of a wormlike chain in a nematic quadrupole field, which can either describe a wormlike chain dissolved in a nematic liquid-crystal medium or a wormlike chain in the self-consistent-field potential due to other chains in the nematic state.[9] In two dimensions, the quadrupole field adds $\beta\mathscr{H}_{\mathrm{ext}} = -\lambda\int_0^L \mathrm{d}s\, ({u_x}^2 - {}^1/_2)$ to the total chain Hamiltonian, where we have chosen the nematic director to be along the x-axis. Since ${u_x}^2 - {}^1/_2 = \cos(2\theta)/2$, the diagrammatic representation for this problem has similar rules to those for the previous two problems, with the exception that the step size in the diagrams is of magnitude 2 instead of 1. Following the same derivation as in the previous problems, we find that the partition function q for a single chain in a nematic quadrupole field is given by

$$q(\Lambda;p) = \cfrac{1}{P_0 - \cfrac{\Lambda^2/8}{P_2 - \cfrac{\Lambda^2/16}{P_4 - \cfrac{\Lambda^2/16}{P_6 - \cfrac{\Lambda^2/16}{\cdots}}}}} \tag{26}$$

where $\Lambda = 2l_p\lambda$. This solution permits the evaluation of a number of thermodynamic properties of a wormlike chain in a nematic field including the chain deformation free energy by the field in two dimensions. It also provides the key input in the self-consistent-field theory for the nematic phase of wormlike chains.

All of the solutions given in this section can be verified by generating moments of the external field by taking derivatives of q with respect to the field strength parameters (K, F, and Λ) evaluated at zero field strength. The solutions can be checked by finding the diagrams that represent these moments, a process that further extends the usefulness of the diagrammatic representation. We find agreement between our solutions and the analytical solutions for the moments of the external field for all cases.

3. Three-Dimensional Solutions

The analogous solutions in three dimensions are found by using virtually identical techniques as those used to find the two-dimensional solutions. We first review the solution of the chain statistics for a wormlike chain in three dimensions in the absence of an external field. The orientation of the tangent vector is defined by the polar angle θ between the tangent and the z-axis and the azimuthal angle ϕ that defines the rotation of the tangent about the z-axis. The Green function $G_0(\vec{u}|\vec{u}_0;L)$ gives the conditional probability that a chain of contour length L beginning with an initial tangent orientation $\vec{u}_0$ will end with tangent orientation $\vec{u}$. As in two dimensions, the Green function is found using the path integral formalism given by

$$G_0(\vec{u}|\vec{u}_0;L) = \int_{\vec{u}(s=0)=\vec{u}_0}^{\vec{u}(s=L)=\vec{u}} \mathscr{D}[\vec{u}(s)] \exp(-\beta\mathscr{H}_0[\vec{u}(s)]) \tag{27}$$

where the path integration includes the spherical angles θ and ϕ. Solving the Schrödinger equation derived from eq 27, the solution for the Green function in three dimensions is given by

$$G_0(\vec{u}|\vec{u}_0;L) = \sum_{l=0}^{\infty} \sum_{m=-l}^{l} {Y_l}^m(\vec{u}) {Y_l}^{m*}(\vec{u}_0) C_l(N) \tag{28}$$

where $C_l(N) = \exp[-l\,(l+1)N]$ $[N = L/(2l_p)]$, and ${Y_l}^m$ are the spherical harmonics.[17]

We begin with the partition function for a chain under tension described by the interaction $\beta\mathscr{H}_{\mathrm{ext}} = -\vec{f}\cdot\int_0^L \mathrm{d}s\, \vec{u}$. We choose our coordinate system so that f lies along the z-axis; thus eq 4 in three dimensions replaces R_x with R_z. As in two dimensions, we make use of the moment-based expansion of eq 4, with some slight modification of the subsequent steps to account for the statistical behavior in three dimensions.

The moment $\langle {R_z}^{2n} \rangle_0$ is found by using orientation statistics with the help of eq 5, where R_x is now replaced with R_z. Because of the "time" ordering in eq 5, the Markovian nature of the tangent vector statistics permits the evaluation of $\langle {R_z}^{2n} \rangle_0$ by insertion of a propagator (eq 28) between each successive factor in the product of eq 5. Since there are $2n+1$ propagators inserted, there are $2n+1$ l-indices and $2n+1$ m-indices to sum over. The initial, final, and intermediate tangent vector orientations ($2n+1$ total) are then integrated over, which selects for certain values of the l-indices and m-indices. The integration over the initial and final tangent orientation selects $l_1 = l_{2n+1} = 0$ and $m_1 = m_{2n+1} = 0$, and upon integration over the intermediate azimuthal angles ϕ_i, the intermediate m-indices are also set to zero. The intermediate selection rules for the l-indices are found by noting that $\cos\theta Y_l^0 = a_{l+1} Y_{l+1}^0 + a_l Y_{l-1}^0$ where $a_l = l/\sqrt{4l^2-1}$,[17] thus the l-indices selected are offset from their neighbors by a value of 1 or −1. Since the l-indices cannot take negative values, the chosen l-indices for $\langle {R_z}^{2n} \rangle_0$ follow paths of $2n$ steps with

unit step size that start at zero and end at zero while never wandering below $l = 0$.

The diagrammatic representation in three dimensions reflects these selection rules. For example, $\langle R_z^2\rangle_0$ in three dimensions contains only 1 l-index path ($l_1 = 0$, $l_2 = 1$, $l_3 = 0$). The three-dimensional version of Figure 1 contains only the first and fifth diagrams in A and the first in lines 1, 3, 4, and 5 and the third in line 5 of B. For the moment $\langle R_z^{2n}\rangle_0$, there are $(2n)!/[n!(n+1)!]$ diagrams that satisfy the selection rules.[10] The value of a given diagram is again most easily stated in Laplace space (with the Laplace variable p): for a diagram corresponding to a particular path $\{l_1, l_2, ..., l_i, ..., l_{2n+1}\}$, the functional value is $P_{l_1}^{-1}\prod_{i=2}^{2n+1} a_{l_i+t_i} P_{l_i}^{-1}$ where $P_l = p + l(l+1)$, and $t_i = 0$ if $l_i = l_{i-1} + 1$ (step up) and $t_i = 1$ if $l_i = l_{i-1} - 1$ (step down). For example, the diagram in three dimensions corresponding to the fifth diagram in A of Figure 1 is given by $P_0^{-1}a_1P_1^{-1}a_2P_2^{-1}a_2P_1^{-1}a_1P_0^{-1}$.

We now construct the diagrammatic representation of the partition function $q(F;p)$. We assign a factor $P_l^{-1} = [p + l(l+1)]^{-1}$ for each l-index and a factor $Fa_{l_i+t_i}$ for a step that connects two adjacent values of the indices l_i and l_{i-1}, where the value of t_i (defined in the previous paragraph) depends on whether the step is up or down. We call these diagrams Fa diagrams. In terms of these diagrams, the partition function can be written as

$$q(F;p) = \text{sum of all Fa diagrams that begin and terminate at } l = 0 \text{ without ever wandering below } l = 0 \tag{29}$$

Following a virtually identical procedure as the two-dimensional analogue for manipulating the diagrams, we obtain the following recursive form for $q(F;p)$:

$$q(F;p) = 1/J_0 \tag{30}$$

where J_n obeys the recursive relation

$$J_n = P_n - a_{n+1}{}^2F^2/J_{n+1} \tag{31}$$

with $P_n = p + n(n+1)$ and $a_n = n/\sqrt{4n^2-1}$. Written as an infinite continued fraction, the partition function now reads

$$q(F;p) = \cfrac{1}{P_0 - \cfrac{a_1{}^2F^2}{P_1 - \cfrac{a_2{}^2F^2}{P_2 - \cfrac{a_3{}^2F^2}{\cdots}}}} \tag{32}$$

The validity of eq 32 can be verified by generating moments of $q(F;p)$ using eq 23. With the expression $\langle R^{2n}\rangle_0 = (2n+1)!\,\langle R_z^{2n}\rangle_0/(2n)!$, our solution provides a convenient method for generating arbitrary moments of the end-to-end distance analytically. As in two dimensions, we have checked our solution by generating moments up to $\langle R^{10}\rangle_0$ and have found exact agreement with the available solutions.[10]

As in two dimensions, the end-to-end distance distribution function in Fourier-Laplace space can be obtained trivially from eq 32 by the substitution $\vec{f} \to i\vec{k}$; the result is

$$G(K;p) = \cfrac{1}{P_0 + \cfrac{a_1{}^2K^2}{P_1 + \cfrac{a_2{}^2K^2}{P_2 + \cfrac{a_3{}^2K^2}{\cdots}}}} \tag{33}$$

where $K = 2l_pk$ and k is the magnitude of $\vec{k}$. We verify that our techniques produce identical results as those given in a previous study[12] by truncating the infinite continued fraction (eq 33) at the third level and finding equivalence between the two solution methods.

A semiflexible chain in the nematic quadrupole field in three dimensions is described by the interaction term $\beta\mathscr{H}_{ext} = -\lambda\int_0^L ds\,(u_z^2 - 1/3)$ in the chain Hamiltonian. Noting that $(\cos^2\theta - 1/3)Y_l^0 = \alpha_{l+2}Y_{l+2}^0 + \beta_lY_l^0 + \alpha_lY_{l-2}^0$ where $\alpha_l = a_{l-1}a_l$ ($a_l = l/\sqrt{4l^2-1}$) and $\beta_l = a_{l+1}{}^2 + a_l{}^2 - 1/3$,[17] we see that the selection rules for this external field includes up and down steps of magnitude 2 as well as horizontal steps. However, the diagrammatic resummation technique discussed earlier can be easily extended to account for this additional horizontal step. The result is

$$q(\Lambda;p) = \cfrac{1}{P_0 - \beta_0\Lambda - \cfrac{\alpha_2{}^2\Lambda^2}{P_2 - \beta_2\Lambda - \cfrac{\alpha_4{}^2\Lambda^2}{P_4 - \beta_4\Lambda - \cfrac{\alpha_6{}^2\Lambda^2}{\cdots}}}} \tag{34}$$

where $P_n = p + n(n+1)$, $\Lambda = 2l_p\lambda$, $\alpha_l = a_{l-1}a_l$ ($a_l = l/\sqrt{4l^2-1}$), and $\beta_l = a_{l+1}{}^2 + a_l{}^2 - 1/3$ (note $\beta_0 = 0$). Equation 34 is equivalently stated as $q(\Lambda;p) = 1/J_0$, where $J_n = P_n - \beta_n\Lambda - \alpha_{n+2}{}^2\Lambda^2/J_{n+2}$ for $n \geq 0$.

We conclude this section by providing a discussion of the similarities between the solutions in two and three dimensions and generalization of our solution methods to a wider range of similar problems. One important conclusion that is evident from our results is that the infinite continued fraction is a natural form for these solutions, which is highly advantageous in its simplicity and its convergence behavior. In deriving our solutions, we have described the formation of the continued fraction as adding layers onto the diagrammatic representation; the use of the diagrammatic techniques provides a means of visualizing our algebraic methods.

The end-to-end distribution function in two dimensions (eq 25) and three dimensions (eq 33) are almost identical with only subtle differences. Consulting the selection rules in two and three dimensions, we see that $a_n = 1/2$ for all n in two dimensions; whereas $a_n = n/\sqrt{4n^2-1}$ in three dimensions. Inserting $a_n = 1/2$ (the two-dimensional case) into eq 33 yields eq 25 with a factor of 2 missing in the first layer of the continued fraction. This difference is due to the selection rules for the m-index of the two-dimensional case: m runs from negative infinity to infinity whereas the l-index of the three-dimensional case runs from zero to infinity.

We clarify this distinction by considering an interesting variant of the end-distribution function. We define $G^{(j)}(k;p)$ as the collection of diagrams that run from j to

j [thus $G(k;p) = G^{(0)}(k;p)$]. In two dimensions, $G^{(j)}(k;p)$ is given by

$$G^{(j)}(k;p) = \frac{1}{\dfrac{K^2/4}{J_{j-1}^{(-)}} + P_j + \dfrac{K^2/4}{J_{j+1}^{(+)}}} \tag{35}$$

where $P_n = p + n^2$, $K = 2l_p k$, and the recursive forms of the continued fractions are given by $J_n^{(+)} = P_n + (K^2/4)/J_{n+1}^{(+)}$ and $J_n^{(-)} = P_n + (K^2/4)/J_{n-1}^{(-)}$ for any value of n. In three dimensions, $G^{(j)}(k;p)$ is given by

$$G^{(j)}(k;p) = \frac{1}{\dfrac{{a_j}^2K^2}{J_{j-1}^{(-)}} + P_j + \dfrac{{a_{j+1}}^2K^2}{J_{j+1}^{(+)}}} \tag{36}$$

where $P_n = p + n(n+1)$, $a_n = n/\sqrt{4n^2-1}$, $K = 2l_p k$, and the recursive forms of the continued fractions are given by $J_n^{(+)} = P_n + (a_{n+1}^2K^2)/J_{n+1}^{(+)}$ ($n \geq 0$), $J_n^{(-)} = P_n + (a_n^2K^2)/J_{n-1}^{(-)}$ ($n \geq 1$), and $J_0^{(-)} = P_0$. The partial continued fractions provide the diagrammatic contributions to $G^{(j)}$ that are above j in the case of $J_{j+1}^{(+)}$ and below j in the case of $J_{j-1}^{(-)}$. We see the three-dimensional solution for $G^{(j)}(k;p)$ differs from the two-dimensional solution since the continued fractions do not extend past the zeroth layer in three dimensions because the l-index in three dimensions take only nonnegative values. The function $G^{(j)}(k;p)$ is necessary in constructing the full end-distribution function including end-tangent orientations, where the diagrams included in the summation have nonzero initial and final m- and l-index values;[10] thus eqs 35 and 36 are important in further extending our current results.

4. Structure Factor of a Wormlike Chain

The single-chain structure factor is one of the most important properties of a polymer. It provides a direct connection to scattering experiments and also the essential theoretical input for treating many-chain systems. While the structure factor for a flexible Gaussian chain model is the well-known Debye function, rigorous results for the structure factor of a semiflexible chain that are valid for arbitrary chain length and persistence length have not been explicitly provided.[18] To date, quantitatively the best available theory for the structure factor for a semiflexible polymer is based on a Dirac equation model proposed by Kholodenko.[19,20] However, this model is designed to smoothly interpolate between the rigid and flexible limits; the extent of its accuracy for intermediate stiffness is not clear. Furthermore, the model cannot be described by a simple Hamiltonian (such as given by eq 1); thus the physical interpretation of its parameters is not straightforward. A variant of the wormlike chain model that permits analytical expressions for the chain statistics involves relaxing the local chain length constraint and enforcing a total chain length constraint instead.[21,22] The accuracy of such a model in predicting the structure factor is questionable due to uncertain contribution of local chain length fluctuations.

In this section, we examine the structure factor of a free wormlike chain for arbitrary chain stiffness using eq 33. We define the structure factor as

$$S(\vec{k}) = \frac{1}{L^2}\int_0^L ds_1 \int_0^L ds_2 \langle \exp[i\vec{k}\cdot(\vec{r}(s_1) - \vec{r}(s_2))]\rangle \tag{37}$$

where the angular brackets indicate an average with respect to the particular chain statistics (in our case wormlike chain in the absence of external fields). Note that this definition differs from the more conventional one by an extra factor of L in the denominator. We choose this dimensionless form in order to simplify our comparison with previous results by Kholodenko.[23,24]

We first recapitulate the structure factors for a Gaussian chain and for a rigid rod. For a chain obeying Gaussian statistics, the scattering function is given by

$$S(\vec{k}) = \frac{1}{L^2}\int_0^L ds_1 \int_0^L ds_2 \exp\left(-\frac{2l_p|s_1 - s_2|\vec{k}^2}{6}\right)$$
$$= \frac{72}{NK^2}\left(\frac{1}{6} - \frac{1 - \exp(-NK^2/6)}{NK^2}\right) \tag{38}$$

where $N = L/(2l_p)$ and $K = 2l_p|\vec{k}|$. We have set the Gaussian step size b to the Kuhn length $2l_p$ to facilitate comparison with the wormlike chain model. For a perfectly rigid chain, the scattering function is given by

$$S(\vec{k}) = \frac{2}{NK}\left(\mathrm{Si}(NK) - \frac{1 - \cos(NK)}{NK}\right) \tag{39}$$

where $\mathrm{Si}(x)$ is the sine integral, defined as $\mathrm{Si}(x) = \int_0^x dz\, \sin(z)/z$. We express eq 39 in terms of NK, which is equal to kL, for ease of comparison with the Gaussian-chain behavior and our current results. We note that as $NK \to \infty$, the structure factor behaves as $S(k) \to \pi/(NK)$.

The structure factor is related to the Green function through

$$S(\vec{k}) = \frac{1}{L^2}\int_0^L ds_1 \int_0^L ds_2\, G(\vec{k}; s_1 - s_2)$$
$$= \frac{2}{N^2}\mathscr{L}^{-1}\left(\frac{G(K;p)}{p^2}\right) \tag{40}$$

where $\mathscr{L}^{-1}$ indicates Laplace inversion from p to N. In two dimensions, $G(K;p)$ in eq 40 is given by eq 25; in three dimensions, it is given by eq 33. Equation 40 is valid for a polymer chain of arbitrary rigidity, provided the Laplace inversion can be accurately performed. All of our numerical results are obtained by truncating the infinite continued fraction at the 20th level and evaluating the inverse Laplace transform by computing residues of the resulting expression numerically. We limit our discussion of the behavior of the structure factor to three dimensions.

Figure 2 shows the behavior of the structure factor (eq 40) in three dimensions for relatively rigid chains [$N = 0.1$ (solid curve), $N = 0.5$ (dashed curve), and $N = 1$ (dashed−dotted curve)]. We plot the product $kLS(k)$ in order to clearly show the asymptotic behavior as $Lk \to \infty$ to be $kLS(k) \to \pi$ regardless of the chain rigidity. The rigid rod solution (eq 39) is also included in Figure 2 (dotted curve) for comparison. We see that as $N \to 0$ the structure factor approaches that for the rigid rod; the two become virtually indistinguishable for $N < 0.02$ (not shown in the figure). The rigid-rod solution exhibits

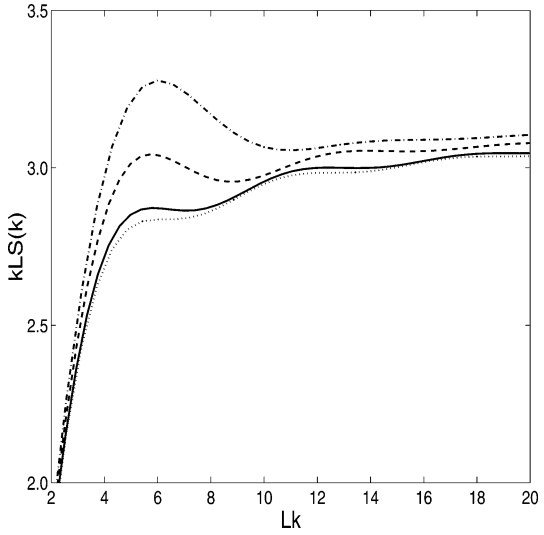

Figure 2. Scattering function $kLS(k)$ vs the wavenumber Lk for $N = 0.1$ (solid curve), $N = 0.5$ (dashed curve), and $N = 1$ (dashed−dotted curve). We include the scattering function for a rigid rod (dotted curve), given by eq 39.

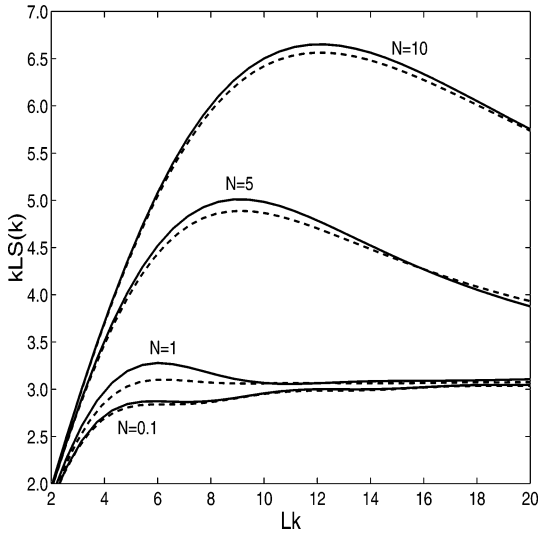

Figure 3. Scattering function $kLS(k)$ vs the wavenumber Lk for $N = 0.1$, $N = 1$, $N = 5$, and $N = 10$ calculated using eq 40 (solid curves) and from solutions found in reference 23 (dashed curves).

an oscillation in $kLS(k)$ when the wavelengths $1/k$ are multiples of the chain lengths L. As the stiffness decreases in Figure 2, the frequency of the oscillations in the structure factor decreases due to the presence of thermal wrinkles in the conformation which shorten the effective length of the chain. In addition, the first peak in $kLS(k)$ emerges dominant as the stiffness decreases, and the subsequent peaks are suppressed because of decreased persistence length.

The behavior of the structure factor for intermediate stiffness is presented in Figure 3 for N ranging from 0.1 (relatively rigid) to 10 (essentially flexible). The dominant peak in the scattering function continues to grow as N increases, and the secondary peaks are no longer noticeable for $N > 1$. For comparison we include in Figure 3 the behavior of the structure factor for a semiflexible chain as defined by Dirac statistics[23,24] (dashed curves). This theory is designed to exactly capture the wormlike chain behavior in the perfectly rigid and flexible limits with an interpolating behavior that captures the wormlike chain behavior in a qualitative manner (see ref 24 for a comparison). Although these two models agree qualitatively, we see in Figure 3 that the wormlike chain model and the Dirac model differ appreciably for semiflexible chains of intermediate stiffness ($N \approx 1$).

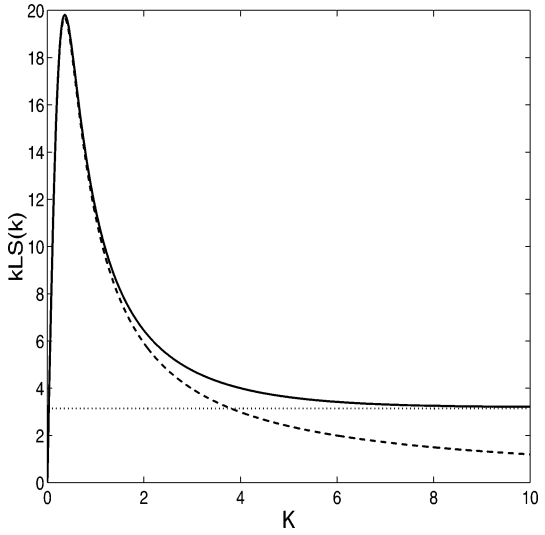

Figure 4. Scattering function $kLS(k)$ vs the wavenumber $K = 2l_pk$ for $N = 100$ for the wormlike chain (solid curve) and the Gaussian chain (dashed curve). The dotted line is the asymptotic value for the wormlike chain $kLS(k) \rightarrow \pi$ as $K \rightarrow \infty$.

As the chain length increases further, the chain becomes more flexible. In Figure 4, we present the scaled structure factor $kLS(k)$ for a chain of length $N = 100$ (solid curve) and compare it with that for a Gaussian chain (dashed curve) given by eq 38. Here we plot $kLS(k)$ against $K = 2l_pk$ since the shortest length scale is now l_p. The dominant peak in Figure 4 occurs when $K \approx 1$, i.e., when the incident wavelength is approximately a Kuhn length $2l_p$. The wormlike chain model closely agrees with the Gaussian chain model for small K; however, as K increases, these two models diverge. Since a wormlike chain is rigid at sufficiently small length scales, the structure factor for the wormlike chain model approaches the rigid rod limit $kLS(k) \rightarrow \pi$ as $k \rightarrow \infty$ regardless of the stiffness of the chain. This limit occurs when $K \gg 1$ for flexible chains ($N \gg 1$) or $kL \gg 1$ for rigid chains ($N \ll 1$). Such behavior is not captured by the Gaussian chain model since a Gaussian chain has no (bending) stiffness at any length scales.

The features of the structure factor illustrated in Figures 2−4 demonstrate the behavior of a wormlike chain ranging from perfectly rigid to flexible. On the rigid side of the spectrum (shown in Figure 2), the structure factor of a wormlike chain becomes essentially indistinguishable from that for the perfectly rigid rod when $N < 0.02$ or when the length of the chain is roughly $^1/_{20}$th of a Kuhn length. However, the difference can be appreciable even for relatively stiff chains ($N \approx 0.1$). This is consistent with the effect of semiflexibility on the thermodynamic behavior of a polymer liquid-crystal solution,[9] where conformation fluctuation substantially alters the nematic−isotropic transition temperature. In the flexible-chain limit (cf. Figure 4), the structure factor for a wormlike chain only coincides with the Gaussian chain result in the small k-limit. The large k-limit of the structure factor, which probes the small length scales of the fluctuating chain, is affected by the bending stiffness of the wormlike chain, which renders

the chain rigid at length scales much less than the persistence length.

5. Polymer Nematics

The formation of a liquid-crystalline phase can be studied at the mean-field level by considering an isolated molecule interacting with an effective self-consistent field that captures the local structure of the ordered phase. In the case of a homogeneous nematic liquid-crystal, the mean-field behavior is captured at the lowest order by a quadrupolar interaction between the molecular orientation and the effective field.[6,7] For semiflexible polymer chains interacting with a Maier−Saupe pseudopotential, the mean-field statistical mechanics of the nematic phase has been solved exactly[8,9] through an expansion of the tangent-vector orientation Green function in the spheroidal functions.[25] However, evaluating the spheroidal functions is a nontrivial mathematical/computational task.

The solutions we provide in this paper for the partition function of a wormlike chain in a quadrupole field provide convenient alternative means for studying a number of important issues involving nematic liquid-crystalline polymers in two and three dimensions. For example, such additional issues include the presence of solvent molecules, both nonmesogenic[9] and mesogenic,[5] and the effect of chain self-assembly on the phase-transition behavior.[26] Regardless of the particular situation, an important input is the behavior of a single semiflexible chain interacting with a quadrupole field.

We thus begin the discussion of the use of our results by considering the thermodynamic behavior of a wormlike chain in an external quadrupole field of strength λ. Focusing on the three-dimensional behavior, the partition function q is given by eq 34, and the Gibbs free energy is given by $\beta g(N;\lambda) = -\log q$. The nematic order parameter, which measures the degree of orientational order is given by

$$m = \frac{1}{L}\int_0^L \mathrm{d}s \left\langle \left(\frac{3}{2}u_z^2 - \frac{1}{2}\right)\right\rangle = \frac{3}{2L}\frac{\partial \log q}{\partial \lambda} \qquad (41)$$

The Helmholtz free energy $f(N;m)$ is then obtained through a Legendre transform as $\beta f(N;m) = \beta g(N;\lambda) + (3/2)\lambda m$. Since both the Gibbs and Helmholtz free energies are defined relative to the isotropic (rotationally invariant) state, the free energy f includes a decrease in the bending energy and a loss of conformation entropy due to alignment by the quadrupole field. We plot the free energy vs the field strength $\Lambda = 2l_p\lambda$ in Figure 5 for $N = L/(2l_p) = 3.3333$.

The free energy in Figure 5 exhibits two distinct scaling regimes. The small Λ scaling of Λ^2 arises from the fact that in the isotropic phase there is no quadrupole order; thus the lowest-order contribution to q must be quadratic in the quadrupole order in the limit of weak field strength. Mathematically, this is seen by noting that $\beta_0 = 0$ in eq 34; thus as $\Lambda \to 0$, the lowest contribution to q is quadratic in Λ. The large Λ scaling can be understood by considering the behavior of the chain conformation in the quadrupole field. In ref 9, we found that the thermodynamic behavior has a distinct crossover when the chain is essentially aligned in the quadrupole field, dictated by suppression of the conformation fluctuations in the direction perpendicular to the quadrupole field. This crossover results in the large Λ scaling of $\Lambda^{1/2}$ exhibited in Figure 5. The thermodynamic behavior demonstrated in Figure 5 captures the free energy of confining a single semiflexible chain in a quadrupole field, regardless of the underlying cause of the field.

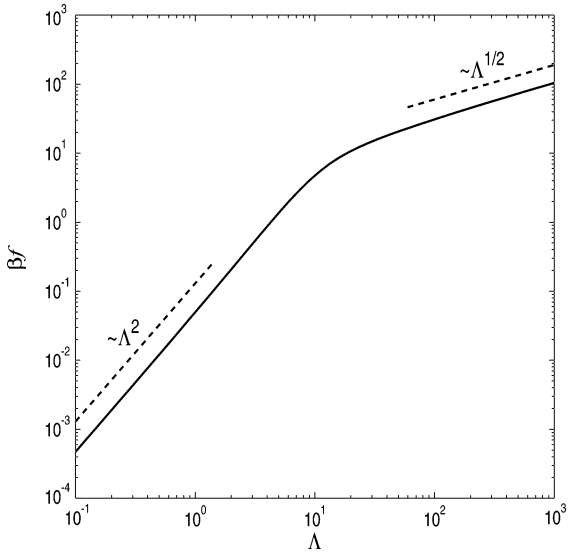

Figure 5. Behavior of the free energy βf vs the quadrupole field strength $\Lambda = 2l_p\lambda$ for $N = L/(2l_p) = 3.3333$ with appropriate scaling behavior for large and small Λ.

We now specify to the mean-field (self-consistent field) treatment of nematic liquid-crystalline polymer phase by replacing the external field with a self-consistent field that approximates the many-body interactions within the nematic phase. The derivation of the full set of self-consistent-field equations is given in ref 9. For simplicity, here we restrict our discussion to the solvent-free thermotropic system. If the strength of the Maier−Saupe interaction is defined to be κ, the self-consistent field is then $\lambda = \kappa m$ and the Helmholtz free energy of the nematic phase relative to the isotropic phase is given by[9]

$$\beta\Delta f = \frac{\kappa L}{3}m^2 - \log q(\kappa m) \qquad (42)$$

The self-consistent calculation of the order parameter m is performed by evaluating eq 42, treating m as a variational parameter and finding values of m that minimize $\beta\Delta f$. The stability of the nematic phase is determined by finding the curvature at the thermodynamically determined value of m. In Figure 6, we show the behavior of the Helmholtz free energy $\beta\Delta f$ vs the order parameter m for $N = L/(2l_p) = 3.3333$ and three different values of κ; these three curves represent the conditions corresponding to the spinodal of the nematic phase, coexistence between the isotropic and nematic phases, and the spinodal of the isotropic phase. When $2l_p\kappa = 20.7582$ (dashed curve), $\beta\Delta f$ has an inflection point at $m = 0.2631$ (indicated by the circle); thus a system initially in the nematic phase becomes unstable with respect to order fluctuations and will spontaneously transform to the thermodynamically favored isotropic phase with $m = 0$ (indicated by the $\times$). By increasing the strength of the nematic interaction to $2l_p\kappa = 21.0606$ (solid curve), we reach coexistence between the isotropic phase with $m = 0$ ($\times$) and nematic phase with $m = 0.3493$ ($\diamond$), where the Helmholtz free energy for the two phases become degenerate. When we increase the nematic interaction further to $2l_p\kappa = 23.6844$,

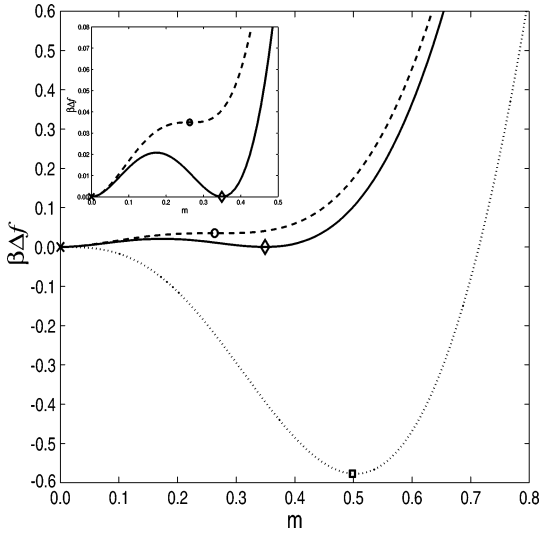

Figure 6. Free energy relative to the isotropic state $\beta\Delta f$ vs the order parameter m for a thermotropic liquid-crystalline polymer system with $N = L/(2l_p) = 3.3333$. When the nematic interaction $2l_p\kappa = 20.7582$ (dashed curve), the nematic phase with $m = 0.2631$ (○) is unstable; thus, the system will spontaneously transition to the isotropic phase with $m = 0$ (×). When $2l_p\kappa = 21.0606$ (solid curve), the isotropic phase (×) is in coexistence with the nematic phase with $m = 0.3493$ (◇). When $2l_p\kappa = 23.6844$ (dotted curve), the isotropic phase (×) spontaneously orders into a nematic phase with $m = 0.4983$ (□). The inset magnifies the behavior near the origin to clarify the coexistence and nematic−spinodal curves.

$\beta\Delta f$ exhibits an inflection point at $m = 0$ (×); thus a system initially in the isotropic phase is unstable with respect to order parameter fluctuations and will spontaneously order to a nematic phase with $m = 0.4983$ (□). The inset of Figure 6 provides a close-up of the dashed and solid curves for clarification.

The results shown in Figure 6 are in full agreement with those obtained in ref 9 using spheroidal functions, thus reaffirming the equivalence between these two approaches. This equivalence implies an interesting mathematical connection between the poles of the continued fraction representation and the eigenvalues of the spheroidal functions, which is worth exploring further.

6. Conclusions

In this work, we present exact, analytical results for the partition function in Laplace space of a single wormlike chain in an external dipole and quadrupole field in two and three dimensions. The results are in the form of infinite continued fractions, which emerge naturally from the hierarchical structure of the diagrammatic techniques employed. The diagrammatic representation, taken from ref 10, provides a visually intuitive means for re-summing the infinite, moment-based expansion of the various partition functions into successive layers. Thus, the rank order of the layers in the continued fraction corresponds to the rank order of layers in the diagrammatic representation.

The greatest appeal of our results is the simplicity and conciseness of the form of the solutions, which makes them easy to use in practical calculations. Because of the rapid convergence of the continued fraction as opposed to simple power series expansions, truncation after a few layers in the infinite continued fraction usually results in sufficient numerical accuracy. For example, the scattering function for a polymer chain in three dimensions with $N = 1$ is accurately captured [less than 1% maximum deviation from the data displayed in Figure 2 ($2 < kL < 20$)] by truncation of the infinite continued fraction at the fourth level.[27] We note that truncation at the nth level exactly reproduces all moments of the distribution function up to the $2n$th moment and approximately captures the higher moments.

The solutions given by eqs 21, 25, 26, 32, 33, and 34 provide the governing equations that are necessary to solve for the end-to-end distance distribution, the structure factor, the response of a chain subject to end tension, and the thermodynamics of nematic liquid-crystalline polymers in two and three dimensions. We have illustrated the use of our results by presenting the exact structure factor of a wormlike chain and the exact mean-field solution for the isotropic−nematic transition in solvent-free semiflexible polymers interacting with a Maier−Saupe type potential. That a number of physical problems involving semiflexible polymers can be addressed by using our results demonstrates their utility.

Acknowledgment. This work was supported in part by the National Science Foundation (DMR-9970589).

References and Notes

(1) Marko, J. F.; Siggia, E. D. *Macromolecules* **1995**, *28*, 8759.
(2) Lamura, A.; Burkhardt, T. W.; Gompper, G. *Phys. Rev. E* **2001**, *6406*, 061801.
(3) Moroz, J. D.; Nelson, P. *Macromolecules* **1998**, *31*, 6333.
(4) Moroz, J. D.; Nelson, P. *PNAS* **1997**, *94*, 14418.
(5) Odijk, T. *J. Chem. Phys.* **1996**, *105*, 1270.
(6) Maier, W.; Saupe, A. *Z. Naturforsch., A* **1958**, *13*, 564.
(7) Maier, W.; Saupe, A. *Z. Naturforsch., A* **1959**, *14*, 882.
(8) Wang, X. J.; Warner, M. *J. Phys. A* **1986**, *19*, 2215.
(9) Spakowitz, A. J.; Wang, Z.-G. *J. Chem. Phys.* **2003**, *119*, 13113.
(10) Yamakawa, H. *Helical Wormlike Chains in Polymer Solutions*; Springer-Verlag: New York, 1997.
(11) Samuel, J.; Sinha, S. *Phys. Rev. E* **2002**, *66*, 050801R.
(12) Stepanow, S.; Schütz, G. M. *Europhys. Lett.* **2002**, *60*, 546.
(13) Temperley, H. N. V.; Lieb, E. H. *Proc. R. Soc. London, Ser. A* **1971**, *322*, 251.
(14) Saito, N.; Takahashi, K.; Yunoki, Y. *J. Phys. Soc. Jpn.* **1967**, *22*, 219.
(15) Feynman, R. P.; Hibbs, A. R. *Quantum Mechanics and Path Integrals*; McGraw-Hill: New York, 1965.
(16) Hermans, J. J.; Ullman, R. *Physica* **1952**, *18*, 951.
(17) Arfken, G. B.; Weber, H. J. *Mathematical Methods for Physicists*; Academic Press: San Diego, CA, 1995.
(18) The study by Stepanow and Schütz[12] mentions the structure factor calculation but does not provide results or discussion.
(19) Kholodenko, A. L. *Ann. Phys.* **1990**, *202*, 186.
(20) Kholodenko, A. L. *J. Chem. Phys.* **1992**, *96*, 700.
(21) Bawendi, M. G.; Freed, K. F. *J. Chem. Phys.* **1985**, *83*, 2491.
(22) Ghosh, K.; Muthukumar, M. *J. Polym. Sci. B* **2001**, *39*, 2644.
(23) Kholodenko, A. L. *Macromolecules* **1993**, *26*, 4179.
(24) Kholodenko, A. L. *Phys. Lett. A* **1993**, *178*, 180.
(25) Meixner, J.; Schäfke, F. M. *Mathieusche Funktionen und Sphäroidfunktionen*; Springer: Berlin, 1954.
(26) Kindt, J. T.; Gelbart, W. M. *J. Chem. Phys.* **2001**, *114*, 1432.
(27) For more rigid chains, accurate calculation of the structure factor requires higher levels of truncation in the continued fraction.

MA049958V